DIRECT AND LARGE EDDY SIMULATIONS OF A BOTTOM EKMAN LAYER UNDER AN EXTERNAL STRATIFICATION

John R. Taylor
Department of Mechanical and Aerospace Engineering,
University of California, San Diego
La Jolla, CA
j2taylor@ucsd.edu

Sutanu Sarkar
Department of Mechanical and Aerospace Engineering,
University of California, San Diego
La Jolla, CA
sarkar@ucsd.edu

ABSTRACT

A steady Ekman layer with a stratified outer layer and an adiabatic lower wall is studied with direct numerical simulation (DNS) and large eddy simulation with a near-wall model (NWM-LES). As the flow evolves from a uniformly stratified initial state, a mixed layer forms near the wall, separated from the outer layer by a strongly stratified thermocline. The thickness of the mixed layer is strongly limited by the outer layer stratification. Observations from the DNS are used to evaluate the LES. The mean velocity profile, mean temperature gradient, and boundary layer height from the LES agree well with the DNS. However, while the LES that is considered here resolves more than 80% of the turbulent kinetic energy away from the wall, it is not able to sufficiently resolve the overturning scales responsible for entrainment at the top of the mixed layer. As a result, the turbulent heat flux and rate of change of the temperature in the mixed layer are significantly underestimated in the LES.

INTRODUCTION

An externally stratified boundary layer forms when a fluid with a stable density stratification flows over an adiabatic surface. Typically, a mixed region forms near the boundary and the thickness of the boundary layer is limited by the external stratification. This situation is nearly ubiqutous at the bottom of the ocean. When the flow is unstratified, the height of a fully-developed rotating boundary layer or Ekman layer scales with $\delta = u_*/f$ where u_* is the friction velocity and f is the Coriolis parameter. Typically in the ocean $\delta = O(100m)$ and the seafloor can be approximated as an adiabatic boundary with the exception of isolated geothermal hotspots. However, the observed boundary layer thickness is often $O(10m)$ indicating that the thickness of the bottom boundary layer is limited by the outer layer stratification.

In the atmosphere, a near-neutral (or conventionally-stable) boundary layer arises when the heat flux at the surface is negligible and the boundary layer height is limited by a thermally stratified inversion layer. This commonly occurs over the surface of the ocean where the surface heat flux tends to be smaller than over land(Businger and Charnock 1983). Based on field observations and simulation results, Grant (1992) found that in the lower portion of a near-neutral atmospheric boundary layer, the dominant balance in the turbulent kinetic energy budget is formed between the production and dissipation, while away from the wall, the turbulent transport terms are non-negligible. Zilitinkevich and Esau (2003) used an LES to simulate the formation of a turbulent Ekman layer with an external stratification and vertical shear, both with and without a surface heat flux. They used their results to formulate a semi-empirical theory for the scaling of the boundary layer height.

Taylor et al. (2005) considered open channel flow with a stablizing heat flux applied at the free surface and an adiabatic lower wall. Under these boundary conditions, a well-mixed turbulent region formed near the lower wall and with a region of stable stratification near the free surface. When the surface heat flux was large, the density difference between the lower mixed layer and the free surface was large enough that the turbulent motions in the bottom boundary layer were unable to lift the dense fluid from the well-mixed region to the free surface. The primary effect of stratification was to limit the turbulent transport away from the wall relative to that observed in the unstratified case.

When a stabilizing heat flux exists at the boundary, as is often the case in nocturnal boundary layers (Mahrt 1999), the effect of stratification is fundamentally different from an externally stratified boundary layer. Armenio and Sarkar (2002) used a LES to study stratified channel flow with a fixed temperature difference across the channel. Owing to the choice of boundary conditions, a heat flux was present near the wall which acted to limit the near-wall turbulent production. The authors found that the simulations using a dynamic mixed model was able to accurately capture the effects of stratification on the bulk flow. In particular, the turbulent Prandtl number increased with the local gradient Richardson number as expected from previous laboratory and numerical studies. A DNS of a stratified Ekman layer with a stabilizing heat flux applied at the lower boundary was considered by Coleman et al. (1992) and Shingai and Kawamura (2002). They found that the boundary layer thickness decreases, and the angle of the surface stress increases with the introduction of stratification.

The goal of the present study is to use numerical simulations to examine the properties of an externally stratified Ekman layer with a particular emphasis on the thermal properties of the boundary layer. Since the role of strat-

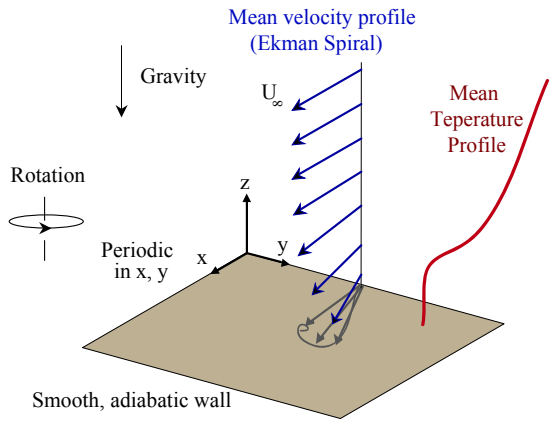

Figure 1: Schematic: Benthic Ekman layer

Table 1: Simulation Parameters

Type	Re_*	Ri_*	(L_x, L_y, L_z)	(N_x, N_y, N_z)
DNS	960	0, 1000	$(2\delta, 2\delta, 2.5\delta)$	$(192, 192, 192)$
LES	960	0, 1000	$(4\delta, 4\delta, 8\delta)$	$(96, 96, 128)$

ification in the near-neutral case is significantly different from that in a stable boundary layer with a heat flux at the boundary, we have conducted a DNS in order to evaluate the performance of an LES at the same Reynolds number. Once confidence in the LES is achieved through a careful comparison with the DNS dataset, simulations can be conducted at a much larger Reynolds number that would more closely approximate the conditions in the ocean and atmosphere.

FORMULATION

A schematic of the flow is shown in Figure 1. The outer flow is in geostrophic balance with a pressure gradient in the y-direction. The bottom wall is a flat, no-slip, adiabatic surface and periodic boundary conditions are applied in the horizontal directions. Near the wall, as viscosity affects the momentum balance, the flow turns in the direction of the pressure gradient, forming a so-called Ekman spiral. Unlike a non-rotating boundary layer, the thickness of an Ekman layer is bounded and scales with $\delta = u_*/f$ when the flow is not stratified. This is an advantage computationally since it is possible to set the domain size to be larger than the boundary layer height, even at long times. When the outer layer flow is stratified, the boundary layer height will be further limited by the influence of stratification. When a stable stratification is present outside of the boundary layer, Taylor and Sarkar (2007) have shown that internal waves are generated by the boundary layer turbulence. In order to allow these waves to freely leave the computational domain, an open boundary condition is approximated using a combination of a radiation condition and a Rayleigh damping region (Klemp and Durran 1983).

Governing Equations

Using the friction velocity, u_*, the turbulent Ekman layer depth, $\delta = u_*/f$, and the outer layer temperature gradient, $d\theta/dz|_\infty$, the nondimensional, spatially filtered governing equations can be written:

$$\frac{\partial \overline{\mathbf{u}}}{\partial t} + \overline{\mathbf{u}}\cdot\nabla\overline{\mathbf{u}} = -\frac{1}{\rho_0}\nabla\overline{p'} + f\widehat{\mathbf{k}}\times(U_\infty\widehat{\mathbf{i}} - \overline{\mathbf{u}}) - Ri_*\overline{\theta'}\widehat{\mathbf{k}} + \frac{1}{Re_*}\nabla^2\overline{\mathbf{u}} - \nabla\cdot\boldsymbol{\tau}, \quad (1)$$

$$\frac{\partial \overline{\theta'}}{\partial t} + \overline{\mathbf{u}}\cdot\nabla\overline{\theta'} = \frac{1}{Re_* Pr}\nabla^2\overline{\theta'} - \nabla\cdot\boldsymbol{\lambda}, \quad (2)$$

$$\nabla\cdot\overline{\mathbf{u}} = 0, \quad (3)$$

where:

$$Re_* = \frac{u_*\delta}{\nu}, \quad Ri_* = -\alpha g\frac{d\theta}{dz}_\infty\frac{\delta^2}{u_*^2} = \frac{N_\infty^2}{f^2}, \quad Pr = \frac{\nu}{\kappa}, \quad (4)$$

u_* is the friction velocity, ν is the molecular kinematic viscosity, κ is the molecular diffusivity, and $\boldsymbol{\tau}$ and $\boldsymbol{\lambda}$ are the subgrid-scale stress and density flux, respectively. The parameters considered in this study are listed in Table 1. Density changes are assumed to be caused by temperature variation in water, motivating the choice of Prandtl number, $Pr = 5$.

NUMERICAL METHOD

Simulations have been performed using a numerical method described in detail in Bewley (2007). Since periodic boundary conditions are applied in the horizontal directions, derivatives in these directions are treated with a pseudo-spectral method. Derivatives in the vertical direction are computed with second order finite differences. Time-stepping is accomplished with a mixed explicit/implicit scheme using third order Runge-Kutta and Crank-Nicolson, respectively. It can be shown that the numerical scheme ensures the discrete conservation of mass, momentum, and energy (Bewely 1999). In order to prevent spurious aliasing due to nonlinear interactions between wavenumbers, the largest 1/3 of the horizontal wavenumbers are truncated using the 2/3 de-aliasing rule (Orszag 1971).

The subgrid scale stress tensor, $\boldsymbol{\tau}$ in Eq. (1) is evaluated using the dynamic mixed model (Zang, Street, and Koseff 1993; Vreman, Geurts, and Kuerten 1997), and a dynamic eddy diffusivity model is used for the subgrid scale density flux, $\boldsymbol{\lambda}$:

$$\tau_{ij} = -2C\overline{\Delta}^2|\overline{\mathbf{S}}|\overline{S_{ij}} + \widehat{\overline{u}_i\overline{u}_j} - \widehat{\overline{u}}_i\widehat{\overline{u}}_j, \quad (5)$$

and

$$\lambda_j = -2C_\theta\overline{\Delta}^2|\overline{\mathbf{S}}|\frac{\partial\overline{\theta}}{\partial x_j}. \quad (6)$$

The Smagorinsky coefficients, C and C_θ are evaluated using the dynamic procedure. This is useful since it avoids an empirical specification of the Smagoinsky coefficient and has been shown to perform well for wall-bounded and density stratified flows (Armenio and Sarkar 2002). The coefficients are evaluated by applying a test filter to the resolved velocity field and using the resolved fields and the test-filtered fields together to estimate the subgrid scale stress and buoyancy flux. Specifically

$$C = \frac{M_{ij}Lij - M_{ij}H_{ij}}{M_{kl}M_{kl}}, \quad (7)$$

where

$$L_{ij} = \widehat{\overline{u_i u_j}} - \widehat{\overline{u}}_i\widehat{\overline{u}}_j, \quad M_{ij} = 2\overline{\Delta}^2\widehat{|\overline{\mathbf{S}}|\overline{S}_{ij}} - 2\widehat{\overline{\Delta}}^2\widehat{|\overline{\mathbf{S}}|}\widehat{\overline{S}_{ij}}, \quad (8)$$

$$H_{ij} = \widehat{\widehat{\overline{u}_i}\widehat{\overline{u}_j}} - \widehat{\widehat{\overline{u}}}_i\widehat{\widehat{\overline{u}}}_j - \left(\widehat{\overline{u}_i\overline{u}_j} - \widehat{\overline{u}}_i\widehat{\overline{u}}_j\right), \quad (9)$$

and

$$C_\theta = \frac{M_i^\theta L^\theta i}{M_j^\theta M_j^\theta}, \quad (10)$$

where

$$L_i^\theta = \widehat{\overline{\theta}\overline{u_i}} - \widehat{\overline{\theta}}\widehat{\overline{u_i}}, \quad M_i^\theta = 2\overline{\Delta}^2|\widehat{\overline{\mathbf{S}}}|\frac{\partial\widehat{\overline{\theta}}}{\partial x_i} - 2\widehat{\overline{\Delta}}^2\widehat{|\overline{\mathbf{S}}|}\frac{\partial\widehat{\overline{\theta}}}{\partial x_i}, \quad (11)$$

The test filter, denoted by $\widehat{\cdot}$, is applied over the horizontal directions only using a trapezoidal rule on a five-point stencil.

A *resolved* LES is usually defined as a simulation that resolves at least 80% of the energy everywhere in the flow (Pope 2000). Near solid boundaries, turbulent motions scale with the viscous scale, $\delta_\nu = \nu/u_*$. Away from boundaries, the largest turbulent eddies are constrained by the domain size, h. Therefore, the ratio of the filter size near the wall to that necessary in the outer layer scales with $\delta_\nu/h = \nu/(u_* h) = 1/Re_*$. Even when considering a stretched grid in the wall-normal direction, this places a strong constraint on the grid spacing for a resolved LES of wall-bounded flows at a large Reynolds number.

In order to allow a lower vertical resolution near the wall, we use a near-wall model in conjunction with the LES. The model that we have used is a modification of that proposed by Schumann(1975), Grotzbach(1987), and Piomelli(1989), and modified slightly for a rotating boundary layer. This model uses an approximate boundary condition for the horizontal velocity near the wall by predicting the wall stress. Since a staggered grid is used in the vertical direction, the wall location is placed at the same location as the vertical velocity. The first horizontal velocity point away from the wall is located at $z^+(1) = 24$ in wall units, and the near-wall grid spacing is $\Delta z^+(1) = 48$. The plane average of the streamwise velocity at the first point away from the wall is then used to estimate the friction velocity by iteratively solving the expected mean logarithmic law:

$$\frac{\langle|\mathbf{u}|\rangle(1)}{u_*} = \frac{1}{\kappa} ln(\frac{z(1)u_*}{\nu}) + B, \quad (12)$$

where $\langle|\mathbf{u}|\rangle(1)$ is the plane averaged horizontal velocity magnitude evaluated at the first gridpoint away from the wall, and we have used $\kappa = 0.41$ and $B = 5.2$. From the friction velocity, the components of the plane-averaged wall stress are estimated by specifying the angle α_0 between the wall-stress and the x-direction:

$$\langle\tau\rangle_{13} = \rho_0 u_*^2 cos(\alpha_0), \quad (13)$$

$$\langle\tau\rangle_{23} = \rho_0 u_*^2 sin(\alpha_0). \quad (14)$$

The local wall stress is then estimated using fluctuations in the resolved horizontal velocity:

$$\tau_{13}(x,y) = \frac{u(x,y,1)}{\langle u\rangle(1)}\langle\tau\rangle_{13}, \quad (15)$$

$$\tau_{23}(x,y) = max(\frac{v(x,y,1)}{\langle u\rangle(1)}\langle\tau\rangle_{13}, \frac{v(x,y,1)}{\langle v\rangle(1)}\langle\tau\rangle_{23}) \quad (16)$$

The latter relation allows a smooth transition between the non-rotating case when the wall stress is dominated by the τ_{13} component and an Ekman layer where the mean velocity and wall stress in the spanwise direction are nonzero.

The grid used by the LES is much coarser than that used in the DNS as shown in Table 1. Near the wall about 60% of the turbulent kinetic energy is resolved by the LES, while more than 80% of the energy is resolved away from the wall, so that these simulations can be categorized as a near-wall model LES (NWM-LES) (Pope 2000). If a DNS was considered with the same domain size as the LES, it would require 80 times more gridpoints than the LES.

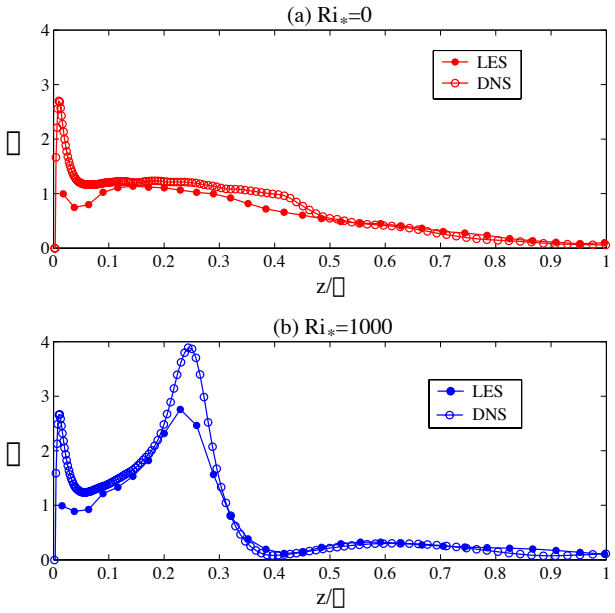

Figure 2: Nondimensional shear, ϕ defined in Eq. (17)

SETUP

We have initialized each simulation with a uniform temperature gradient corresponding to the external stable stratification and a velocity field taken from an unstratified simulation at steady state. The initial evolution of the flow is only simulated using LES since a long time DNS would be prohibitively expensive. After the flow is initialized, a thermally well-mixed region forms near the wall. Eventually the flow reaches a quasi-steady state and the mixed layer exhibits a slow linear growth in time. At about $20/f$ time units after initializing the temperature profile (at a latitude of 45^o, this corresponds to 54 hours), the DNS is started by interpolating the LES velocity and temperature field onto the higher resolution grid. Each DNS is then allowed to evolve for approximately $t = 3/f$ time units.

RESULTS

Mean velocity profile

Before examining the performance of the LES in simulating the thermal structure of the boundary layer, it is useful to examine the mean velocity profiles. In constructing the near-wall model for the LES, we have made the assumption that the stratified and unstratified simulations obey the same logarithmic law. Since gridpoints near the wall are within the well-mixed layer, this seems reasonable, but it should be tested using the DNS results. Figure 2 shows the vertical shear normalized by the expected shear in the log-region:

$$\phi = \frac{\kappa z}{u_*}\left(\frac{d\langle u\rangle}{dz}^2 + \frac{d\langle v\rangle}{dz}^2\right)^{1/2}. \quad (17)$$

Based on this definition, when $\phi = 1$ the mean shear is in agreement with the expected value from the logarithmic law. As seen in Figure 2(a), the mean shear in the unstratified

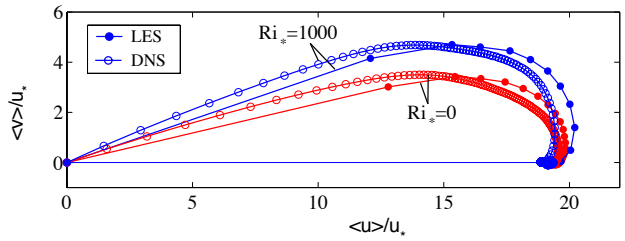

Figure 3: Hodograph of the mean velocity

DNS follows the logarithmic law scaling for approximatley $0.05 \leq z/\delta \leq 0.3$ and the LES is able to reproduce this behavior. Figure 2(b) shows that there is a small region, $0.05 < z/\delta < 0.1$, where the stratified Ekman layer also has $\phi \approx 1$. Therefore, it appears to be appropriate to assume that the mean shear follows the unstratified logarithmic law at a point next to the wall, as has been done in the near-wall model. The mean shear increases dramatically in the thermocline when $Ri_* = 1000$. The LES is able to capture some of this increase, but the maximum shear is not as large as in the DNS. Since the resolution of this LES is quite low, it is not too surprising that it is unable to fully resolve the sharp gradients in this region.

The individual components of the mean horizontal velocity are shown in Figure 3. As has been observed for an Ekman layer with a stabilizing surface heat flux, the presence of an outer layer stratification acts to increase the cross-stream velocity. It is interesting to note that the angle of the Ekman spiral increases near the wall where the mean temperature gradient is zero. Therefore, the effect of stratification in this region appears to be non-local. The LES is able to generally capture the increase in the Ekman transport when the outer layer is stratified, although $< v > /u_*$ is slightly underestimated near the wall and $< u > /u_*$ is overestimated in the outer layer compared to the DNS results.

Thermal field

Since the lower wall is adiabatic and the molecular diffusion of heat is small, the heat content of the boundary layer is approximately conserved. In addition, at some location far enough from the boundary layer, the mean temperature profile is unchanged from its initial state. As a result, when the temperature profile mixes near the wall, the temperature gradient must increase above the mixed layer in order to return the temperature to the initial state. When the flow is strongly stratified, the region with a nonzero turbulent heat flux is limited by stratification. In this case, the temperature gradient is very large in a thermocline above the mixed layer. The mean temperature field in the stratified boundary layer can then be characterized by a three-layer structure with a well-mixed region near the wall, a strongly stratified thermocline, and an outer layer were the temperature gradient is equal to the initial value. This structure can be seen in the plane-averaged temperature gradient in Figure 4(b).

When $Ri_* = 0$, we still consider a uniform temperature gradient in the outer layer, but since the thermal and momentum equations become decoupled, the temperature is advected as a passive scalar. This allows us to evaluate the performance of the LES model in describing both passive and active scalar mixing. The mean temperature gradient from the LES and DNS compares favorably both when the temperature is treated as a passive scalar as well as in the

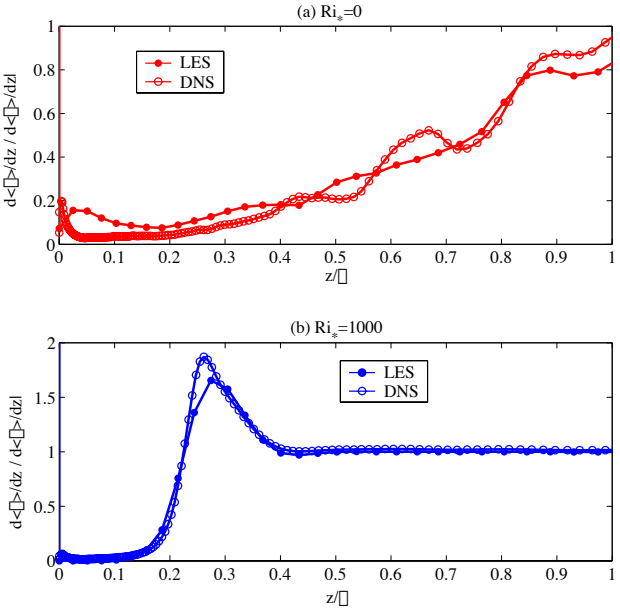

Figure 4: Mean temperature gradient normalized by outer value

stratified simulations as seen from Figure 4.

An important difference between the DNS and LES results is that the LES significantly underestimates the rate of entrainment of outer layer fluid into the mixed layer. This can be quantified by comparing the rate of increase of the temperature of the mixed layer fluid. When the flow is strongly stratified and $Ri_* = 1000$, the rate of change of the mixed layer temperature integrated between the wall and 0.1δ is more than a factor of two lower in the LES compared to the DNS, 0.0018 and 0.0042, respectively, in units of $d\langle\theta\rangle/dz|_\infty \delta^2 * f$. When $Ri_* = 0$ and temperature acts as a passive scalar, the LES entrainment rate shows better agreement with the DNS and the rate of change of the integrated mixed layer temperature is 0.0085 for the LES compared to 0.0112 for the DNS.

The evolution of the mean temperature field can be written in terms of the molecular and turbulent heat flux:

$$\frac{\partial\langle\theta\rangle}{\partial t} = \frac{\partial}{\partial z}\left(\kappa\frac{\partial\langle\theta\rangle}{\partial z} - \langle\theta' w'\rangle\right). \qquad (18)$$

The right hand side of Eq. (18) is dominated by the turbulent heat flux in the mixed layer and by the molecular heat flux above the thermocline. Since the heating of the mixed layer fluid is underpredicted by the LES, particularly when $Ri_* = 1000$, it follows that the estimate of the turbulent heat flux is also low as shown in Figure 5. In both cases, the subgrid-scale contribution is shown by a dashed line. Evidently, when $Ri_* = 0$ nearly all of the heat flux is accounted for by the resolved scales, while the subgrid-scale heat flux is very important when $Ri_* = 1000$, particularly in the lower half of the mixed layer.

A visualization of the temperature field from the DNS with $Ri_* = 1000$ is shown in Figure 6. In the mixed layer, small scale overturns and filaments are visible. Since the vertical grid spacing in the LES at the top of the mixed layer is about 0.03δ, many of the small scale features are not resolved by the LES. Outside of the mixed layer, the characteristic scale of the temperature fluctuations increases dramatically. In the outer layer, stratification is strong enough to suppress turbulence, and an internal wave field is induced by

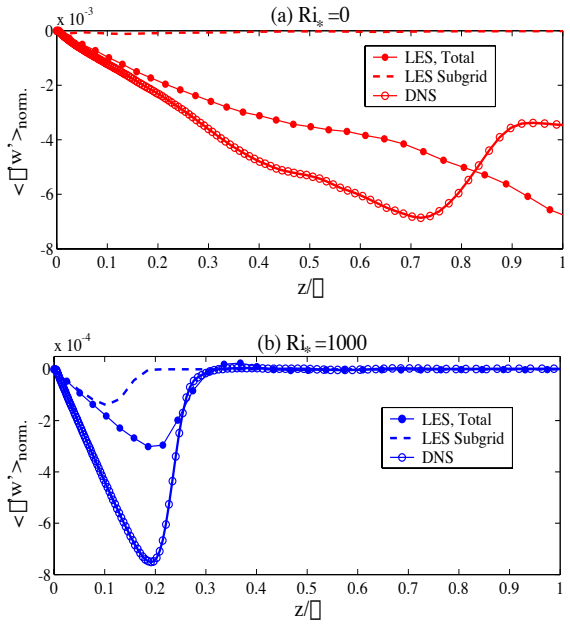

Figure 5: Turbulent heat flux normalized by $d < \theta > /dz|_\infty \delta u_*$

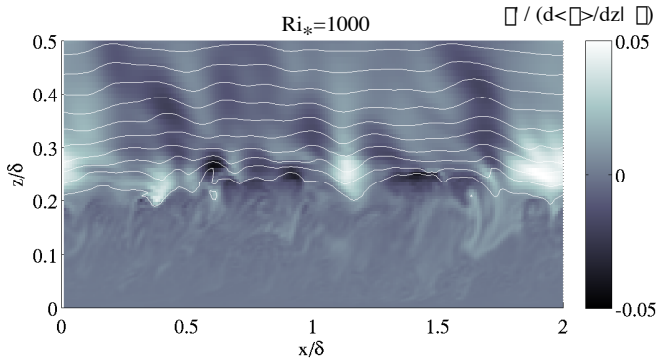

Figure 6: Instantaneous visualization of the temperature field from DNS with $Ri_* = 1000$. Perturbations from the plane mean are shown in shades of gray, and white lines indicate isoterms.

the boundary layer turbulence.

The horizontal scales in the $\langle \theta' w' \rangle$ field are visualized in a horizontal plane located at $z = 0.2\delta$ (the location of maximum turbulent heat flux) in Figure 7 for the DNS and a subset of the LES domain. At this location, $\langle \theta'^2 \rangle$ is nearly the same in the DNS and LES and $\langle v'^2 \rangle$ is actually larger in the LES. As we have seen, however, the magnitude of $< \theta' w' >$ is underpredicted by the LES. In Figure 7, it is apparent that many of the small scale features are not present in the LES and the number of regions with a negative heat flux is higher in the DNS. Since the LES is unable to resolve all of the scales, and the subgrid-scale heat flux is negligible at this height, the LES underestimates the plane averaged turbulent heat flux.

The length scale associated with density overturns can be estimated by the Ellison scale:

$$L_E = \frac{(\theta'^2)^{1/2}}{d\langle\theta\rangle/dz}. \tag{19}$$

In the DNS at $Ri_* = 1000$, at $z = 0.2\delta$, the Ellison scale is $L_E = 0.03\delta$. At this location, the LES gridspacing is

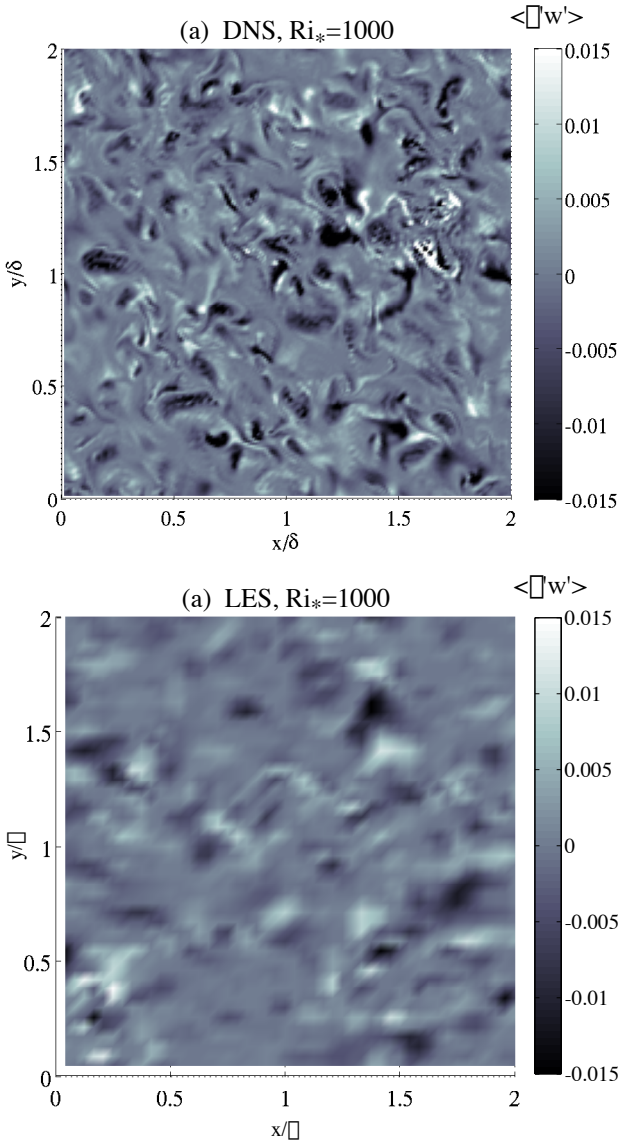

Figure 7: Instantaneous visualization of the turbulent heat flux at $z/\delta = 0.2$, $Ri_* = 1000$

$(\Delta_x, \Delta_y, \Delta_z) = (0.04\delta, 0.04\delta, 0.03\delta)$ which will not sufficiently resolve the density overturns. Therefore, the LES is unable to resolve or model all scales responsible for the turbulent entrainment at the top of the mixed layer.

The turbulent Prandtl number, defined as the ratio of the turbulent viscosity and diffusivity can be written:

$$Pr_T = \frac{\nu_T}{\kappa_T} = \frac{\left(\langle u'w'\rangle^2 + \langle v'w'\rangle^2\right)^{1/2}}{-\langle\theta'w'\rangle} \frac{d\langle\theta\rangle/dz}{d\langle u\rangle/dz}. \tag{20}$$

Given that the LES underestimates the turbulent heat flux in the mixed layer when $Ri_* = 1000$, it is surprising that the turbulent Prandtl number is also lower than the DNS in this case as seen in Figure 8. In both the stratified and unstratified DNS, the mixed region is characterized by $Pr_T \approx 1$ as has been reported for turbulence in a low stratification environment (Schumann and Gerz 1995). The low value of the turbulent Prandtl number near the wall in the LES is directly related to an underestimate of the mean temperature gradient. In the DNS, the temperature gradient only vanishes in a thin viscous layer near the wall, consistent with the observations using a *resolved* LES by Taylor et al. (2005). In

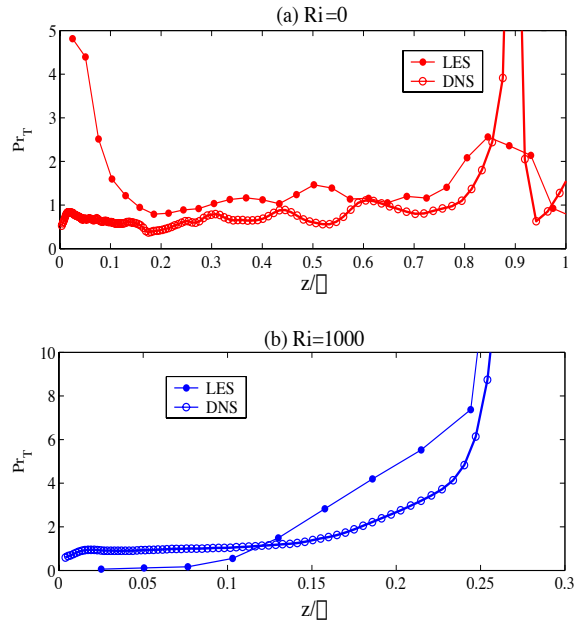

Figure 8: Turbulent Prandtl number

the current LES with a low near-wall resolution, the temperature gradient is much smaller near the wall. For example, at $z/\delta = 0.05$, the temperature gradient normalized by the outer layer value is $d\langle\theta\rangle/dz = 8*10^{-4}$ in the LES, compared to $d\langle\theta\rangle/dz = 1.6*10^{-2}$ in the DNS. This is consistent with the observation that the LES is not able to account for the full variability of the temperature field in the mixed layer.

CONCLUSIONS

We have conducted simulations of an Ekman layer formed when a steady, linearly stratified fluid flows over a smooth boundary in the absence of a surface heat flux. When the initial stratification is strong, the boundary layer thickness is limited by stratification. A DNS was used to examine evaluate the performance of a near-wall model LES with an emphasis placed on the thermal structure of the boundary layer. We have found that the mean velocity and the mean temperature gradient compare well between the DNS and LES. However, the turbulent heat flux in the boundary layer is significantly underpredicted by the LES. Flow visualizations revealed that small scale motions that are not resolved by the LES or represented in the subgrid-scale model are responsible for the entrainment of fluid into the boundary layer in the DNS. When $Ri_* = 0$ and the temperature is decoupled from the momentum equations, the turbulent heat flux from the LES agrees more closely with the DNS. In this case, entrainment into the boundary layer is dominated by larger scales which are fully resolved by the LES.

*

References

Armenio, V. and S. Sarkar (2002). An investigation of stably stratified turbulent channel flow using large-eddy simulation. *J. Fluid Mech. 459*, 1–42.

Bewely, T. (1999). *Optimal and robust control and estimation of transition, convection, and turbulence*. Ph. D. thesis, Stanford University.

Bewely, T. (2007). *Numerical methods for simulation, optimization, and control*.

Businger, J. and H. Charnock (1983). Boundary layer structure in relation to larger scale flow: some remarks on the jasin observations. *Phil. Trans. R. Soc. Lond. A 308*, 445–449.

Coleman, G., J. Ferziger, and P. Spalart (1992). Direct simulation of the stably stratified turbulent ekman layer. *J. Fluid Mech. 244*, 677–712.

Grant, A. (1992). The structure of turbulence in the near-neutral atmospheric boundary layer. *J. Atmos. Sci. 49*(3), 226–239.

Grotzbach, G. (1987). Direct numerical and large eddy simulation of turbulent channel flows. In N. Cheremisinoff (Ed.), *Encyclopedia of Fluid Mechanics*, Volume 6, pp. 1337–1391. West Orange, NJ: Gulf Publ.

Klemp, J. and D. Durran (1983). An upper boundary condition permitting internal gravity wave radiation in numerical mesoscale models. *Monthly Weather Review 111*, 430–444.

Mahrt, L. (1999). Stratified atmospheric boundary layers. *Boundary-Layer Meteorology 90*, 375–396.

Orszag, S. (1971). Numerical simulation of incompressible flows within simple boundaries. 1. galerkin (spectral) representation. *Stud. Appl. Maths L*, 293.

Piomelli, U., J. Ferziger, P. Moin, and J. Kim (1989). New approximate boundary conditions for large eddy simulations of wall-bounded flows. *Phys. Fluids A 1*(6), 1061–1068.

Pope, S. (2000). *Turbulent Flows*. Cambridge: Cambridge University Press.

Schumann, U. (1975). Subgrid-scale model for finite difference simulation of turbulent flows in plane channels and annuli. *J. Comp. Phys. 18*, 376–404.

Schumann, U. and T. Gerz (1995). Turbulent mixing in stably stratified shear flows. *Journal of Applied Meteorology 34*, 33–48.

Shingai, K. and H. Kawamura (2002). Direct numerical simulation of turbulent heat transfer in the stably stratified ekman layer. *Thermal Science and Engineering 10*, 25.

Taylor, J. and S. Sarkar (2007). Internal gravity waves generated by a turbulent bottom ekman layer. *Submitted to J. Fluid Mech.*.

Taylor, J., S. Sarkar, and V. Armenio (2005). Large eddy simulation of stably stratified open channel flow. *Physics of Fluids 17*, 116602.

Vreman, B., B. Geurts, and H. Kuerten (1997). Large-eddy simulation of the turbulent mixing layer. *J. Fluid Mech. 339*, 357–390.

Zang, Y., R. Street, and R. Koseff (1993). A dynamic mixed subgrid-scale model and its application to turbulent recirculating flows. *Phys. Fluids A 5*(12), 3186–3196.

Zilitinkevich, S. and I. Esau (2003). The effect of baroclinicity on the equilibrium depth of neutral and stable planetary boundary layers. *Q.J.R. Meteorological Society 129*, 3339–3356.